Dielectric Ribbon Waveguide: An Optimum Configuration for Ultra-Low-Loss Millimeter/Submillimeter Dielectric Waveguide

C. YEH, FELLOW, IEEE, FRED I. SHIMABUKURO, MEMBER, IEEE, AND J. CHU, STUDENT MEMBER, IEEE

Abstract—**Dielectric ribbon waveguide supporting the $_eHE_{11}$ dominant mode can be made to yield an attenuation constant for this mode of less than 20 dB/km in the millimeter/submillimeter-wavelength range. The waveguide is made with a high-dielectric-constant, low-loss material such as alumina or sapphire. It takes the form of thin dielectric ribbon surrounded by lossless dry air. A detailed theoretical analysis of the attenuation and field extent characteristics for the low-loss dominant $_eHE_{11}$ mode along a ribbon dielectric waveguide was carried out using the exact finite-element technique as well as two approximate techniques. Analytical predictions were then verified by measurements on ribbon guides made with Rexolite using the highly sensitive cavity resonator method. Excellent agreement was found.**

I. INTRODUCTION

THE PHENOMENAL success of the dielectric fiber as an ultra-low-loss optical waveguide has enticed us to reconsider the viability of the dielectric rod as a low-loss millimeter/submillimeter (mm/sub-mm) waveguide. A survey of commercially available materials shows that two classes of material may be excellent candidates as low-loss dielectric materials for mm/sub-mm wave applications [1]–[6]: (1) crystalline material such as quartz, alumina, and sapphire and (2) nonpolar polymers such as poly-4-methylpentene-1 (TPX), PTFE (Teflon), polyethylene (LDPE), and polypropylene. Another way to minimize the attenuation constant for the guided wave along a dielectric structure is to use special waveguide configurations. This paper will first provide a brief survey of commercially available low-loss dielectric material and highlight possible ways to reduce the loss factor. Then we will focus our attention on identifying low-loss configurations. It is shown that a properly configured waveguide can support the dominant mode with a loss factor as much as 50–100 times below that for an equivalent circular dielectric waveguide. A loss factor of less than 20 dB/km can be realized with presently available material. This waveguide takes the form of a thin dielectric ribbon surrounded by lossless dry air. Theoretical analyses have been carried out based on three approaches: the slab approach [7], Marcatili's approach [8], and the exact finite-element approach [9]. Experimental verification of selected cases has also been carried out using the unique ultra-high-Q dielectric waveguide cavity resonator apparatus that we developed [10]. Our investigation shows that it is feasible to design a long-distance mm/sub-mm wave communication line with losses approaching 20 dB/km using the dielectric ribbon waveguide made with commercially available low-loss, high-dielectric-constant material.

Manuscript received December 8, 1988; revised February 18, 1990. This work was supported in part by the UCLA–TRW MICRO Program and by the U.S. Air Force under Contract F04701-87-C-0088.

C. Yeh and J. Chu are with the Electrical Engineering Department, UCLA, Los Angeles, CA 90024-1594.

F. I. Shimabukuro is with the Aerospace Corporation, P.O. Box 92957, Los Angeles, CA 90009.

IEEE Log Number 9035405.

II. A DISCUSSION ON LOW-LOSS DIELECTRIC MATERIAL

A series of very detailed measurements in the mm/sub-mm wavelength range on the dielectric constants and loss tangents of groups of promising low-loss materials has been performed by the MIT "Mag-Lab" group in recent years. Results of their findings were summarized in a very comprehensive paper by Afsar and Button [1]. Afsar [3] also presented his measured results on several very low loss nonpolar polymers. A sample list of two types of commercially available low-loss materials is given in Table I. It can be seen that the polymer material in general has a much lower dielectric constant than the crystalline material. The best loss tangent is of the order of 10^{-4}. Using a nominal dielectric constant of 2.0, the attenuation constant for plane wave in this bulk material is 1.3 dB/m at 100 GHz, which is already better than the 2.4 dB/m loss for conventional metallic waveguides at this frequency. The attenuation constant for plane wave is calculated from the following equation [11]:

$$\alpha = 8.686\left(\pi\sqrt{\epsilon_r}/\lambda_0\right)\tan\delta \quad (\text{dB/m}). \tag{1}$$

Here ϵ_r is the relative dielectric constant, λ_0 is the free-space wavelength, and $\tan\delta$ is the loss tangent. According to (1), it appears that in addition to requiring as small a loss tangent as possible, a lower dielectric constant is also helpful in achieving lower loss. Hence, flexible nonpolar polymers such as LDPE (polyethylene) and

0018-9480/90/0600-0691$01.00

TABLE I

Crystalline Material [4]–[6]	Dielectric constant	Loss tangent
ZnS (at 100 GHz)	8.4	2×10^{-3}
Alumina (at 10 GHz)	9.7	2×10^{-4}
Sapphire (at 100 GHz)	9.3–11.7	4×10^{-4}
Quartz (at 100 GHz)	3.8–4.8	5×10^{-4}
KRS-5 (at 94.75 GHz)	30.5	1.9×10^{-2}
KRS-6 (at 94.75 GHz)	28.5	2.3×10^{-2}
$LiNbO_3$ (at 94.75 GHz)	6.7	8×10^{-3}
Polymer Material [1]–[3]	Dielectric constant	Loss tangent
Teflon (at 100 GHz) (PTFE)	2.07	2×10^{-4}
Rexolite (at 10 GHz)	2.55	1×10^{-3}
RT-Duroid 5880 (at 10 GHz)	2.2	9×10^{-4}
Polyethylene (at 100 GHz) (LDPE)	2.306	3×10^{-4}
TPX (Poly-4 methylpentene-1) (at 100 GHz)	2.071	6×10^{-4}
Polypropylene (at 100 GHz)	2.261	7×10^{-4}

PTFE (Teflon) may be good choices for making low-loss mm/sub-mm waveguides. However, this conclusion can be deceiving because it is based purely on the low-loss property of the waveguide material; i.e., only bulk material loss is considered and the effect of waveguide configuration on losses has not been included. If the configuration effect is taken into account, material with lower dielectric constant may not offer the advantage of lower attenuation constant as indicated by (1). (Detailed consideration will be given to this in Section III.)

One way to construct low-loss waveguide material is to use an artificial dielectric [12], [13]. The artificial dielectric may be composed of alternate longitudinal layers of low-loss, high-dielectric-constant material such as quartz and air. One may also interpret this approach as a way of altering the configuration of guided wave structure, which will be addressed in the next section. The artificial dielectric material may also be constructed with small particles (size $\ll \lambda_0$) of low-loss, high-dielectric-constant material such as small quartz or sapphire spheres suspended in air. For example, the dielectric constant and loss tangent of sapphire at 100 GHz are 10 and 4×10^{-4}, respectively. Roughly speaking, if a volume contains 10% sapphire powder (small spheres), the equivalent dielectric constant would be approximately 2, and the equivalent loss tangent could be reduced to 4×10^{-5}. Thus high-dielectric-constant, low-loss crystalline materials are excellent candidates for the construction of artificial low-loss dielectric materials.

Returning to our discussion of polymers, it is known that the molecules that make up a typical molecular crystal are bound together by strong valence forces and are held in their correct places in the lattice by much weaker van der Waals forces. The major absorption mechanisms in nonpolar polymers in the mm/sub-mm region are [3]:

1) resonances of normal modes of macromolecular helices;
2) absorption spectrum of impurities such as catalyst residues, antioxidants, ionic impurities, plasticizers, catalyst residues, and other additives;
3) amorphous behavior of polymers.

Recognizing the mechanisms that are generally responsible for the absorption spectra of these polymers in the mm/sub-mm/far-infrared region, one may selectively improve the loss characteristics of a given polymer. For example, impurities may be controlled and reduced; other ions may be introduced to stiffen the long chain molecules so that the chain-twisting vibrations in the mm-wave frequencies may be dampened, reducing the absorptions at these frequencies; and the amorphous characteristics of the polymer can be altered by using different cooling/melting processes.

It will be shown in the following section that a high-dielectric-constant material with low loss tangent is the preferred material for the construction of specially configured ultra-low-loss waveguides.

III. Low-Loss Configuration Study

Reducing the loss tangent of the bulk material will certainly improve the attenuation constant of a guided wave along a dielectric waveguide made with such material. It appears that other major factors that can influence the attenuation characteristics of guided wave along a dielectric structure are the size and shape of the waveguide. The attenuation constant for a dielectric waveguide with arbitrary cross-sectional shape is given by the following expression [11]:

$$\alpha = 8.686\pi(1/\lambda_0)(L_1 + L_0) \qquad (\text{dB/m}) \qquad (2)$$

where

$$L_{1,0} = (\epsilon_{1,0}) \tan \delta_{1,0} R_{1,0} \qquad (3)$$

$$R_{1,0} = \left| \frac{\int_{A_{1,0}} (\boldsymbol{E}_{1,0} \cdot \boldsymbol{E}^*_{1,0})\, dA}{\sqrt{\frac{\mu}{\epsilon}} \left[\int_{A_1} \boldsymbol{e}_z \cdot (\boldsymbol{E}_1 \times \boldsymbol{H}_1^*)\, dA + \int_{A_0} \boldsymbol{e}_z \cdot (\boldsymbol{E}_0 \times \boldsymbol{H}_0^*)\, dA \right]} \right|. \qquad (4)$$

Here, the subscripts 1 and 0 refer, respectively, to the core region and the cladding region of the guide, $\epsilon_{1,0}$ and $\tan\delta_{1,0}$ are, respectively, the relative dielectric constant and the loss tangent of the dielectric material, λ_0 is the free-space wavelength, ϵ and μ are, respectively, the

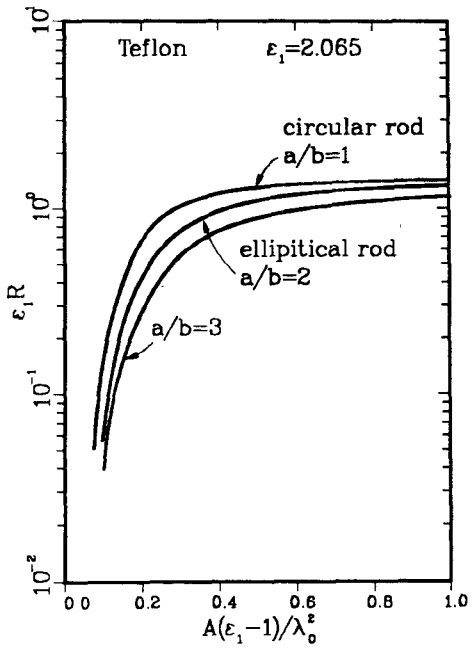

Fig. 1. Configuration loss factor $\epsilon_1 R$ as a function of normalized frquency for an elliptical Teflon rod supporting the dominant ${}_eHE_{11}$ mode. Here A is the cross-sectional area, λ_0 is the free-space wavelength, a is the semimajor axis of the elliptical rod, and b is the semiminor axis. Note that flatter rod yields a smaller configuration loss factor for the same cross-sectional area.

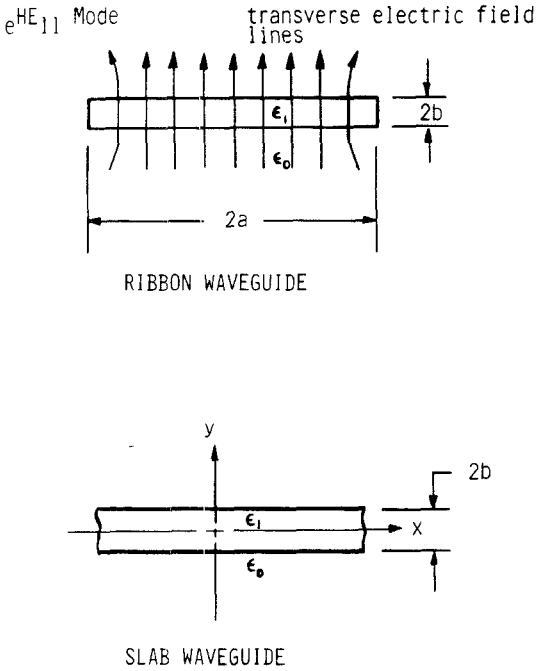

Fig. 2. Cross-sectional geometries for ribbon waveguide and slab waveguide.

permittivity and permeability of free space, e_z is the unit vector in the direction of propagation, A_1 and A_0 are, respectively, the cross-sectional areas of the core and the cladding region, and $\boldsymbol{E}$ and $\boldsymbol{H}$ are the electric and magnetic field vectors of the guided mode under consideration.

If the core and cladding regions contain similar dielectric material, as in the case of optical fiber waveguide, the attenuation constant α will be relatively insensitive to the geometry of the guide because $(R_1 + R_0)$ will be insensitive to the geometry of the guide. For this case, the attenuation of the wave is determined totally by the loss tangent of the material, and the guide configuration is unimportant. On the other hand, if the cladding region (region 0) contains low-loss dry air or is a vacuum, then the loss factor $\epsilon_1 R_1$, which is sensitive to the guide configuration and the frequency of operation, will play an important role in determining the attenuation constant of the mode guided by the dielectric structure. This loss factor $\epsilon_1 R_1$ could vary from a very small value to $\sqrt{\epsilon_1}$, which is the case for a plane wave propagating in a dielectric medium with relative dielectric constant ϵ_1. So, for a given operating frequency, the smaller the factor $\epsilon_1 R_1$, the more desirable the configuration. As an example, the $\epsilon_1 R_1$ factors for an elliptical Teflon dielectric waveguide supporting the dominant ${}_eHE_{11}$ mode as a function of the normalized cross-sectional area for different (major axis)/(minor axis) ratios are given in Fig. 1. It is seen that a mere flattening of a circular dielectric rod along the maximum intensity of the electric field lines for the dominant ${}_eHE_{11}$ mode can improve the $\epsilon_1 R_1$ factor (hence, α) by a factor of 2 or more [11]. It appears that flattening the circular dielectric rod tends to redistribute and spread out the electric field intensities in such a way that the factor $\int_{A_1}(\boldsymbol{E}_1 \cdot \boldsymbol{E}_1^*)\,dA$ in (4) (hence, α) is substantially reduced. This deduction leads us to the conclusion that a very flat elliptical cylinder or simply a thin ribbon may be an extremely attractive low-loss configuration.

A. Wave Guidance Along a Dielectric Slab

Let us now turn our attention to the problem of wave guidance by an infinite flat plate as shown in Fig. 2. Two types of dominant modes may exist on this structure: the TM mode (with E_y, E_z, H_x), which is the low-loss mode, and the TE mode (with H_y, H_z, E_x), which is the high-loss mode. The field components for these modes are given below [7], [12]. (Since only the symmetric modes are considered, the following field expressions, applicable in the region $y > 0$, are used.)

TM Wave: In region 1 (the core region),

$$E_y^{(1)} = \frac{-j\beta}{p_1} B \cos p_1 y$$

$$E_z^{(1)} = B \sin p_1 y$$

$$H_x^{(1)} = \frac{-j\omega\epsilon_1\epsilon}{p_1} B \cos p_1 y \tag{5}$$

and in region 0 (the cladding region),

$$E_y^{(0)} = \frac{-j\beta}{p_0} C e^{-p_0 y}$$

$$E_z^{(0)} = C e^{-p_0 y}$$

$$H_x^{(0)} = \frac{-j\omega\epsilon_0\epsilon}{p_0} C e^{-p_0 y} \tag{6}$$

with

$$k_0^2 = \omega^2\mu\epsilon_0\epsilon \qquad k_1^2 = \omega^2\mu\epsilon_1\epsilon$$

$$p_0^2 = \beta^2 - k_0^2 \quad \text{and} \quad p_1^2 = k_1^2 - \beta^2.$$

TE Wave: In region 1 (the core region),

$$H_y^{(1)} = \frac{j\beta D}{p_1}\cos p_1 y$$

$$H_z^{(1)} = D\sin p_1 y$$

$$E_x^{(1)} = \frac{j\omega\mu D}{p_1}\cos p_1 y \tag{7}$$

and in region 0 (the cladding region),

$$H_y^{(0)} = \frac{j\beta}{p_0}Fe^{-p_0 y}$$

$$H_z^{(0)} = Fe^{-p_0 y}$$

$$E_x^{(0)} = \frac{j\omega\mu}{p_0}Fe^{-p_0 y}. \tag{8}$$

We have assumed that the expressions for the field components of all modes are multiplied by the factor $\exp(j\omega t - j\beta z)$, which will be suppressed throughout. Here β and ω are, respectively, the propagation constant and angular frequency of the wave, and z is the direction of propagation of the wave. Matching the tangential electric and magnetic fields at the boundary surface $y = b$ yields the dispersion relations for the symmetric TM and TE modes, from which the $\omega - \beta$ characteristics for these modes may be found. The dispersion relations and the ratios of unknown coefficients are as follows.

TM Wave:

$$\tan p_1 b = \frac{\epsilon_1}{\epsilon_0}\frac{p_0 b}{p_1 b} \qquad p_1^2 + p_0^2 = k_0^2\left(\frac{\epsilon_1}{\epsilon_0} - 1\right)$$

$$\frac{B}{C} = \frac{e^{-p_0 b}}{\sin p_1 b}. \tag{9}$$

TE Wave:

$$\tan p_1 b = \frac{p_0 b}{p_1 b} \qquad p_1^2 + p_0^2 = k_0^2\left(\frac{\epsilon_1}{\epsilon_0} - 1\right)$$

$$\frac{D}{F} = \frac{e^{-p_0 b}}{\sin p_1 b}. \tag{10}$$

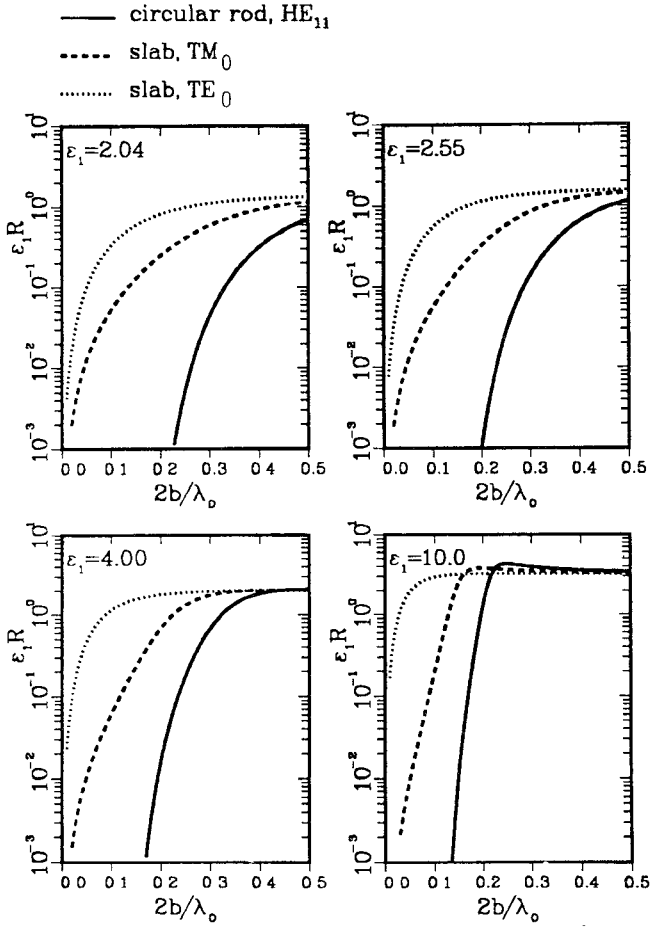

Fig. 3. Configuration loss factor $\epsilon_1 R$ as a function of normalized frequency for a dielectric slab of thickness $2b$ supporting the dominant TE_0 and dominant TM_0 modes and for a circular rod of radius b supporting the dominant HE_{11} mode for various dielectric materials.

Referring to (4), one may also calculate the configuration loss factor R as follows:

$$R^{(\mathrm{TM})} = \frac{(p_0 b)^3}{2(p_1 b)(k_0 b)(\beta b)} \cdot \frac{\left[2p_1 b\left(1 + \left(\frac{\beta b}{p_1 b}\right)^2\right) - \left(1 - \left(\frac{\beta b}{p_1 b}\right)^2\right)\sin 2p_1 b\right]}{\left[\frac{1}{2}\left(\frac{p_0 b}{p_1 b}\right)^3\frac{\epsilon_1}{\epsilon_0}(2p_1 b + \sin 2p_1 b) + \sin^2 p_1 b\right]} \tag{11}$$

$$R^{(\mathrm{TE})} = \frac{1}{2}\frac{k_0 b}{\beta b}\left(\frac{p_0 b}{p_1 b}\right)^3 \cdot \frac{(2p_1 b + \sin 2p_1 b)}{\left[\left(\frac{p_0 b}{p_1 b}\right)^3\frac{1}{2}(2p_1 b + \sin 2p_1 b) + \sin^2 p_1 b\right]}. \tag{12}$$

As expected, one can easily show the limiting case for $R^{(\mathrm{TE})}$ and $R^{(\mathrm{TM})}$ as $(2b/\lambda_0) \to \infty$; it is

$$R^{(\mathrm{TE})} = R^{(\mathrm{TM})} \to 1/\sqrt{\epsilon_1}.$$

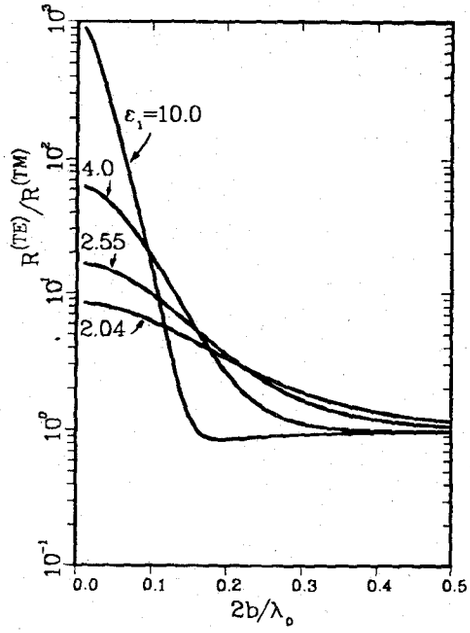

Fig. 4. Ratio of the configuration loss factor for TE_0 and TM_0 versus the normalized frequency for various dielectric materials. Note that the effect of higher dielectric constant material on the ratio is much more pronounced.

Although $R^{(TM)}$ and $R^{(TE)}$ approach the same limit as $2b/\lambda_0$ approaches ∞, the behavior of $R^{(TM)}$ versus $2b/\lambda_0$ and that of $R^{(TE)}$ versus $2b/\lambda_0$ are very different. Fig. 3 gives plots of $\epsilon_1 R^{(TM)}, \epsilon_1 R^{(TE)}$ versus $2b/\lambda_0$ for different values of ϵ_1. The normalized coefficient $R^{(TM),(TE)}\epsilon_1$ is used because it is proportional to the attenuation constant $\alpha^{(TM),(TE)}$. For a given $2b/\lambda_0$ and $\epsilon_1, \epsilon_1 R^{(TM)}$, in general, is significantly lower than $\epsilon_1 R^{(TE)}$, indicating that the dominant TM_0 mode is the low-loss mode. The ratios of $[\epsilon_1 R^{(TE)}]/[\epsilon_1 R^{(TM)}]$ versus $2b/\lambda_0$ for three values of ϵ_1 are shown in Fig. 4. It is of interest to note that the ratio is higher for higher ϵ_1. For example, at the nominal operating frequency of $2b/\lambda_0 = 0.1$, when $\epsilon_1 = 2.04$ (Teflon), the ratio $\epsilon_1 R^{(TE)}/\epsilon_1 R^{(TM)}$ is 6; when $\epsilon_1 = 2.55$ (Rexolite), the ratio is 10; and when $\epsilon_1 = 4$ (quartz) the ratio is 19, indicating that the loss factor for the TM_0 mode is 19 times smaller than that for the TE_0 mode for material with a higher dielectric constant. This fact appears to suggest that high-dielectric-constant material with low loss tangent is the most desirable material for low-loss dielectric waveguides.

Since the field guided along a dielectric waveguide without cladding material extends into the region beyond the dielectric core, it is of interest to learn the relationship between the loss factor $\epsilon_1 R$ and the field extent beyond the core region. In Fig. 5, the loss factor $\epsilon_1 R$ is plotted against the normalized field extent beyond the core surface, expressed by the distance d from the core surface at which the power density of the guided mode has decayed to $1/e$ of its value at the core surface divided by the free-space wavelength. So, given $\epsilon_1 R$ and ϵ_1, one may obtain the normalized distance from the core surface at which the guided power has decayed to its $1/e$ value at

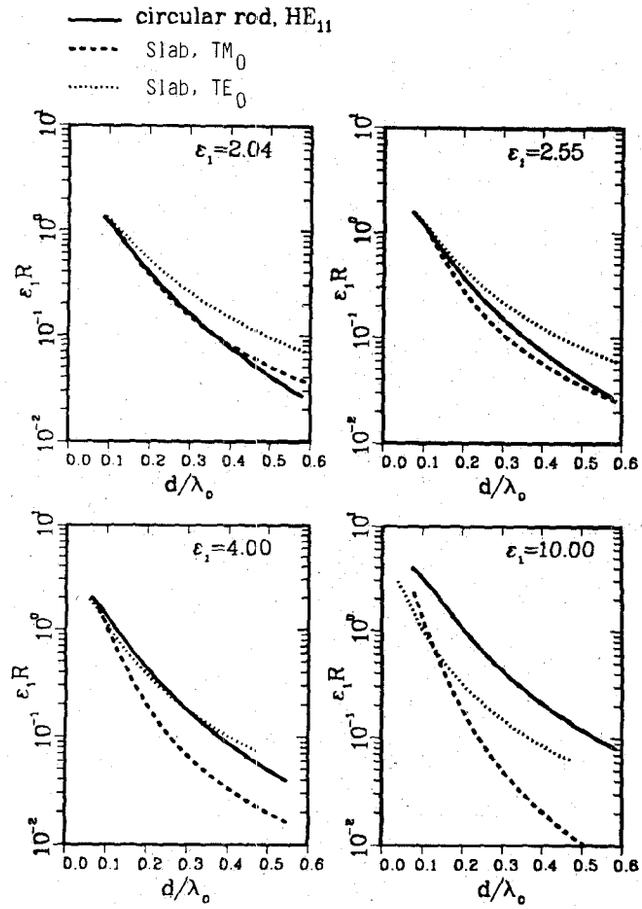

Fig. 5. Configuration loss factor $\epsilon_1 R$ as a function of normalized power decaying distance d/λ_0. Here d is the $1/e$ power decaying distance from the surface of the slab or rod, as appropriate. Note that for high-dielectric-constant materials, the power decaying distance is much shorter for a slab guide than that for a circular rod guide for the same configuration loss factor.

the core surface. For example, if $\epsilon_1 R$ is 0.1 and $\epsilon_1 = 4.0$ (quartz), $d/\lambda_0 = 0.26$ for the low-loss TM_0 mode on a slab, $d/\lambda_0 = 0.38$ for the HE_{11} mode on a circular rod, and $d/\lambda_0 = 0.41$ for the high-loss TE mode on a slab.

B. Wave Guidance Along a Dielectric Ribbon

Recognizing the fact that the dominant ${}_e HE_{11}$ mode guided along a flat dielectric ribbon with aspect ratio greater than, say, 10 must behave similarly to the dominant TM_0 mode guided along a dielectric slab and that the only significant differences must be due to the fringing fields at the edges of the flat ribbon guide, one may make use of the slab results to obtain the approximate results for the ${}_{e,o} HE_{11}$ modes along a dielectric ribbon guide with high aspect ratio. It is also expected that at very low frequencies, because of the large field extent around the guiding structure, implying that the field pattern for an infinite plate would be substantially different from that for a ribbon structure, the loss factor behavior for infinite plate and ribbon will also be very different. This very low frequency region would not be the region of interest because the mode is too loosely guided for any

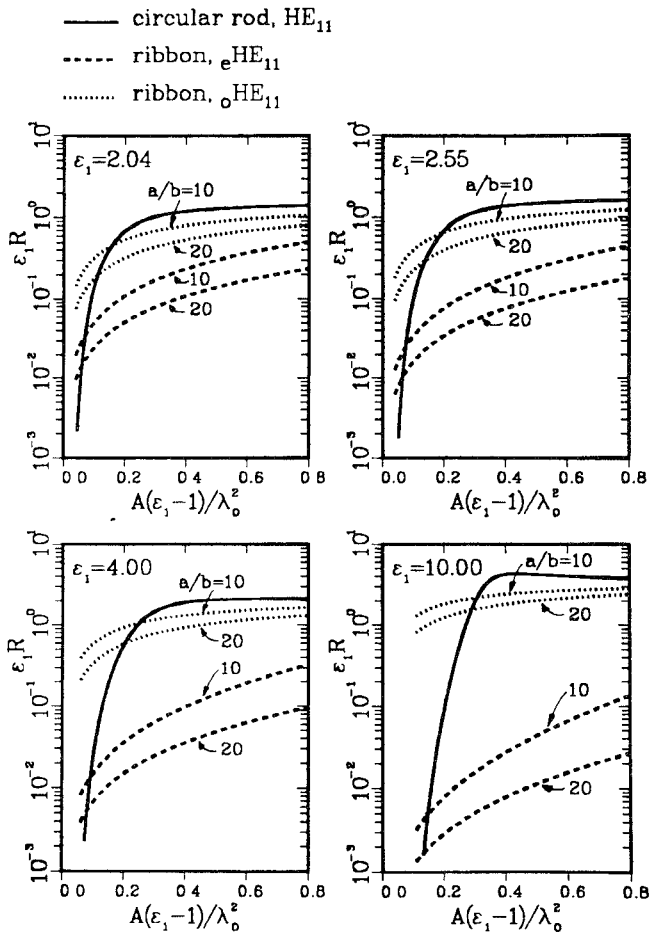

Fig. 6. Configuration loss factor $\epsilon_1 R$ as a function of normalized frequency for a dielectric ribbon with width $2a$ and thickness $2b$ for various dielectric materials. This calculation is based on the slab approximation for which all fields external as well as internal are confined within a width of $2a$. Note, for a given normalized frequency, the dramatic difference between the configuration loss factor for a ribbon supporting the low-loss TM wave and that for a circular rod supporting the HE_{11} mode, especially for higher dielectric constant material.

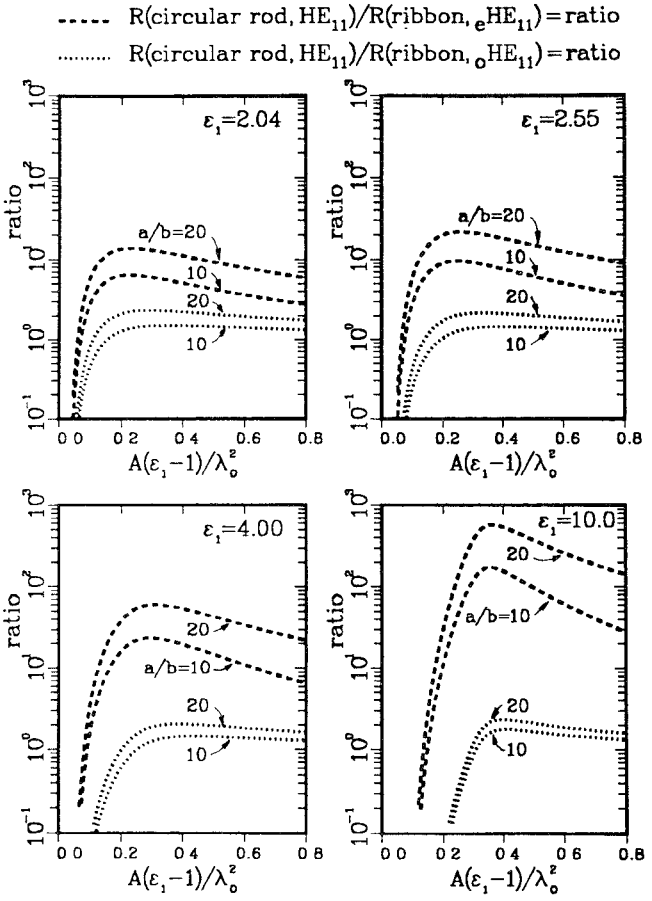

Fig. 7. Ratio of the configuration loss factor for circular rod and ribbon versus the normalized frequency for ribbon of various aspect ratios and for different dielectric materials. Note that for $\epsilon_1 = 10$ and $a/b = 20$, the ratio at $A(\epsilon_1 - 1)/\lambda_0^2 = 0.35$ is as high as 600.

practical applications. The loss factor $\epsilon_1 R$ is plotted against the normalized area, $A(\epsilon_1 - 1)/\lambda_0^2$, where A is the cross-sectional area of the guide, in Fig. 6. It can be seen that there is a dramatic difference between the loss factors for the ribbon TM ($_eHE_{11}$) mode, the ribbon TE ($_oHE_{11}$) mode, and the circular rod HE_{11} mode for the same normalized area. The loss factor for flat ribbon guide supporting the $_eHE_{11}$ mode could be as much as 100 times smaller than that for a circular rod guide supporting the HE_{11} mode. Furthermore, for a rather broad region of normalized area, the loss factor, $\epsilon_1 R$, is reasonably flat for the ribbon guide while it is rather steep for a circular rod guide, indicating that the ribbon guide possesses rather stable low-loss behavior for any possible fluctuation in operating frequencies or cross-sectional area changes.

Another way of demonstrating the advantage of ribbon guide over circular rod guide is shown in Fig. 7, where the loss factor ratio, $\epsilon_1 R$ (for circular rod)/$\epsilon_1 R$ (for ribbon), is plotted against the normalized cross-sectional area. Again, a dramatic difference is seen. For example, from Fig. 7 with $\epsilon_1 = 10$ (sapphire), if the normalized area is 0.35, the ratio could be as high as 400 for a ribbon with aspect ratio of 20:1, indicating that the loss factor for a ribbon guide could be as much as 400 times less than that for a circular rod. These curves also show the advantage of using high-dielectric-constant and low-loss-tangent material to construct the waveguide structure. Fig. 8 demonstrates this.

A major concern of any open guiding structure is the field extent outside the core region. The fact that the loss factor for a flat ribbon can be made so much smaller than that for an equivalent circular rod is primarily due to the spreading of the guided power in the lossless outer (non-core) region. But the distinguishing feature of a ribbon guide is its expanding surface area, which enables the guided mode to attach to it. This feature is very much unlike the case for the circular rod, which possesses very minimal surface area; hence, its guided mode (in the low-loss region) tends to be loosely attached to the guide and can easily detach itself and become a radiated wave. How rapidly the power density of the guided mode decays from the core surface is shown in Fig. 9 for the four low-loss guiding materials. In this figure, the normalized distance, d/λ_0, is plotted against the normalized area.

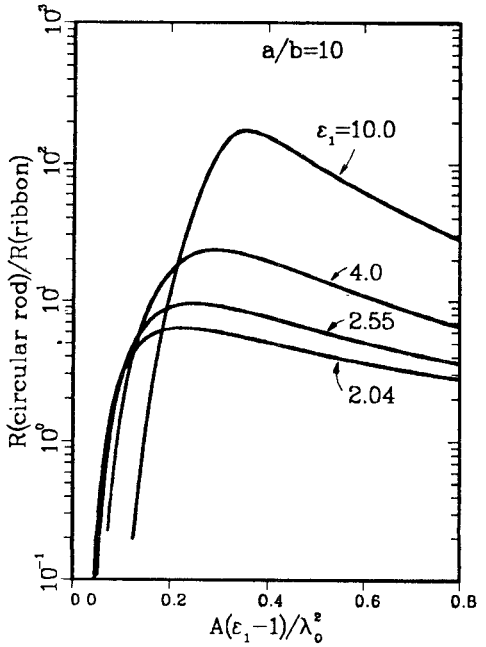

Fig. 8. Ratio of the configuration loss factor for circular rod and ribbon versus the normalized frequency for ribbon with an aspect ratio of 10 for various dielectric materials. Note the dramatic increase of the ratio as ϵ_1 is increased.

Here, d is the distance from the core surface at which the power density of the guided mode has decayed to $1/e$ of its value at the core surface. For a typical operating range $(0.2 \leqslant A(\epsilon_1 - 1)/\lambda_0^2 \leqslant 1.0)$, the normalized field extent, d/λ_0, is less than 0.5. In other words, it is safe to conclude that most of the guided power is confined within a region whose outer boundary is situated at least one free-space wavelength away from the core boundary. For millimeter or submillimeter operation, this requirement is easily accommodated.

IV. Theoretical Verifications

In the previous section, the solution for a plane slab is used to form the solution for a ribbon with high aspect ratio. Further refinement of the slab solution can be obtained using an approximate approach developed by Marcatili [8]. He formulated an approximate solution to the problem of wave guidance by rectangular dielectric structures by ignoring the matching of fields along the corners of the rectangular dielectric structure. By matching the tangential electric and magnetic fields along the four sides of the rectangular core region, and assuming that the field components in the core region vary sinusoidally in the two transverse directions along its major and minor axes (those in upper and lower regions outside the core varying sinusoidally along the direction for the major axis and decaying exponentially along the direction for the minor axis, and those in the left and right regions outside the core varying sinusoidally along the direction for the minor axis and decaying exponentially along the direction for the major axis), one may obtain a dispersion relation from which the propagation constants of various modes may be calculated. For the low-loss TM wave, the propagation constant β can be found by solving the following equations:

$$2ak_x = \pi - 2\tan^{-1}\left[k_x/\left(k_1^2 - k_0^2 - k_x^2\right)^{1/2}\right]$$

$$2bk_y = \pi - 2\tan^{-1}\left[\left(k_y/\epsilon_1\right)/\left(k_1^2 - k_0^2 - k_y^2\right)^{1/2}\right]$$

$$\beta^2 = k_1^2 - k_x^2 - k_y^2. \tag{13}$$

Here, $2b$ and $2a$ are, respectively, the height and the width of the ribbon guide; $k_1^2 = \omega^2\mu\epsilon_1\epsilon$ and $k_0^2 = \omega^2\mu\epsilon_0\epsilon$. The configuration loss factor $R_{\text{Marcatili}}^{(\text{TM})}$ is

$$R_{\text{Marcatili}}^{(\text{TM})} = |I|/\left[\sqrt{\mu/\epsilon}\,|I_p|\right] \tag{14}$$

with

$$\begin{aligned} I = {} & (\omega\epsilon_1\beta)^{-2}ab\Big\{(k_xk_y)^2\left[1-\operatorname{sinc}(2k_xa)\right] \\ & \cdot\left[1-\operatorname{sinc}(2k_yb)\right] \\ & +\left(k_1^2-k_y^2\right)^2\left[1+\operatorname{sinc}(2k_xa)\right]\left[1+\operatorname{sinc}(2k_yb)\right] \\ & +(\beta k_y)^2\left[1+\operatorname{sinc}(2k_xa)\right]\left[1-\operatorname{sinc}(2k_yb)\right]\Big\} \end{aligned}$$

$$\begin{aligned} I_p = {} & \left(k_1^2-k_y^2\right)ab(\omega\epsilon_1\beta)^{-1}\left[1+\operatorname{sinc}(2k_xa)\right] \\ & \cdot\left[1+\operatorname{sinc}(2k_yb)\right] \\ & +\left(k_1^2-k_y^2\right)a(\omega\epsilon_0\beta)^{-1} \\ & \cdot\left(k_1^2-k_0^2-k_y^2\right)^{-1/2}\left[1+\operatorname{sinc}(2k_xa)\right]\cos^2(k_yb) \\ & +\left(k_0^2-k_y^2\right)b(\omega\epsilon_0\beta)^{-1}\left(k_1^2-k_0^2-k_x^2\right)^{-1/2} \\ & \cdot\cos^2(k_xa)\left[1+\operatorname{sinc}(2k_yb)\right]. \end{aligned}$$

To compare the configuration loss factors $R_{\text{Marcatili}}^{(\text{TM})}$ with $R^{(\text{TM})}$ (according to the slab model), Fig. 10 is introduced. In this figure the normalized configuration loss factors for both models are plotted against the normalized area. It is seen that, for a normalized frequency larger than 0.1 and $b/a > 3$, the loss factors for both models are quite close to each other, indicating that the slab model approximation approaches Marcatili's approximation. One also observes that as the aspect ratio increases for the rectangular dielectric waveguide, as expected, the loss factor based on Marcatili's approximation approaches that based on the slab model. The fact that Marcatili's curves are above the slab model curves is worth noting; it means that the nonuniform distribution of the electric field intensity within the rectangular core region tends to increase the configuration loss factor. This conclusion is consistent with our previous conjecture that achieving a uniform distribution of the electric field intensity within the core region promotes the low-loss behavior of the guided mode. Hence, flat ribbon with high aspect ratio appears to be the optimal configuration in achieving a low loss factor.

The above results, shown in Fig. 10, reaffirm the validity of the slab model in providing a good theoretical guideline for designing ultra-low-loss ribbon dielectric waveguides.

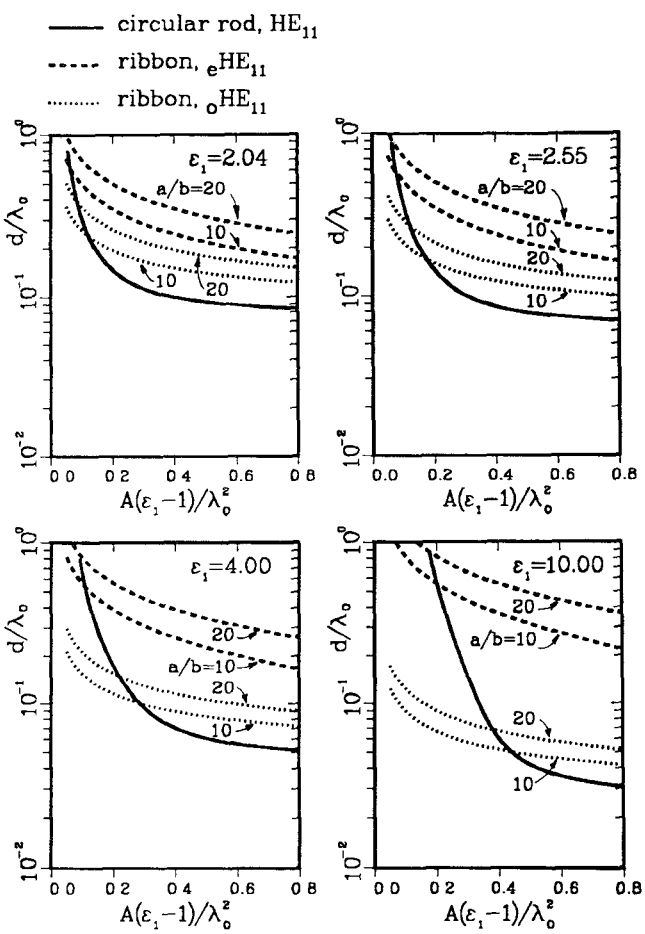

Fig. 9. Normalized power decaying distance d/λ_0 as a function of normalized frequency for various ribbon aspect ratios and for different dielectric materials. Here d is the $1/e$ power decaying distance from the surface of the ribbon or rod. Note that for all regions of interest (i.e., $0.2 < A(\epsilon_1 - 1)\lambda_0^2 < 0.8$), d is less than one free-space wavelength

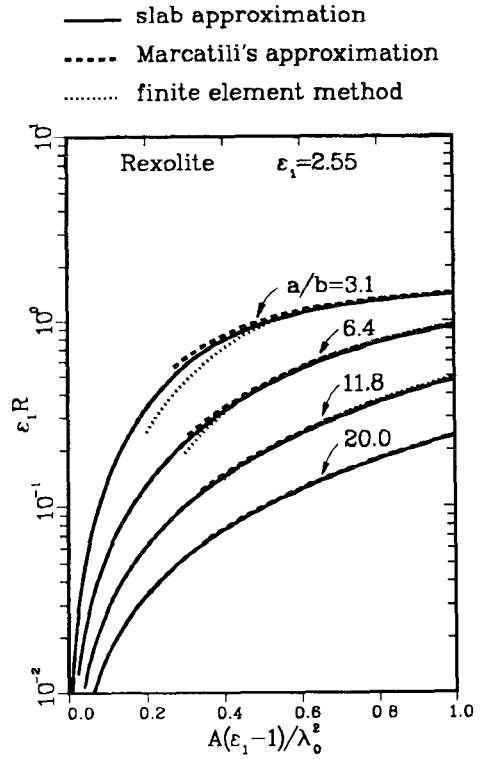

Fig. 10. Configuration loss factor versus normalized frequency for the dielectric ribbon waveguide. Results are obtained according to two approximate methods: the slab approximation and Marcatili's approximation, and one exact method: the finite element method. Within the region of interest, i.e., $0.3 < A(\epsilon_1 - 1)/\lambda_0^2 < 2.0$, results from approximate methods agree very closely with those from the exact method for flat ribbon with $a/b \geq 10$, where $2a$ is the width and $2b$ is the thickness of the ribbon; only when $a/b < 6.4$ are the differences noticeable. This graph shows that the approximation approaches can be used with confidence to predict the configuration loss factor behavior for thin ribbons.

To further validate the slab model, an exact approach based on the solution of Maxwell's equations by the finite element approach is used to calculate the configuration loss factor. According to this finite element approach [9], the governing longitudinal fields of the guided wave are first expressed as a functional as follows:

$$I = \sum_{p=1} I_p$$

$$= \sum_{p=1} \iint \left\{ \tau_p |\nabla H_z^{(p)}|^2 + \gamma^2 \tau_p \epsilon_p \left| \frac{1}{\gamma} \left(\frac{\epsilon_0}{\mu} \right)^{1/2} \nabla E_z^{(p)} \right|^2 + 2\gamma^2 \tau_p \hat{e}_z \cdot \left[\frac{1}{\gamma} \left(\frac{\epsilon_0}{\mu} \right)^{1/2} \nabla E_z^{(p)} \times \nabla H_z^{(p)} \right] - \left(\frac{\omega}{c} \right)^2 (\gamma^2 - 1) \left[(H_z^{(p)})^2 + \gamma^2 \frac{\epsilon_p}{\epsilon_0} \cdot \left[\frac{1}{\gamma} \left(\frac{\epsilon_0}{\mu} \right)^{1/2} E_z^{(p)} \right]^2 \right] \right\} dx\,dy \quad (15)$$

where

$$\gamma = \frac{\beta c}{\omega} \qquad \tau_p = \frac{\gamma^2 - 1}{\gamma^2 - \epsilon_p}.$$

Here ϵ_p is the dielectric constant in the pth region, $\hat{e}_z$ is a unit vector in the z direction, and c is the speed of light in vacuum. The symbol p represents the pth region when one divides the guiding structure into appropriate regions. Minimizing the above surface integral over the whole region is equivalent to satisfying the wave equation and the boundary conditions for E_z and H_z. In the finite element approximation, the primary dependent variables are replaced by a system of discretized variables over the domain of consideration. Therefore, the initial step is a discretization of the original domain into many subregions. For the present analysis, there are a number of regions in the composite cross section of the waveguide for which the permittivity is distinct. Each of these regions is discretized into a number of smaller triangular subregions interconnected at a finite number of points, called nodes. Appropriate relationships can then be developed to represent the waveguide characteristics in all triangular subregions. These relationships are assembled into a system of algebraic equations governing the entire

cross section. Taking the variation of these equations with respect to the nodal variable leads to an algebraic eigenvalue problem from which the propagation constant for a certain mode may be determined. The longitudinal electric field, $E_z^{(p)}$, and the longitudinal magnetic field, $H_z^{(p)}$, in each subdivided pth region are also generated in this formalism. All transverse fields in the pth region can subsequently be produced from the longitudinal fields. A complete knowledge of the fields can be used to generate the configuration loss factor according to (4). Results are also shown in Fig. 10, where the configuration loss factors for four rectangular ribbon guides with aspect ratios of 3.1, 6.4, 11.8, and 20 are plotted as a function of their normalized areas. In the same figure, results based on the slab model, as well as on Marcatili's approximation, are also given. It is seen that when the aspect ratio is 3.1 the curve based on the exact analysis is substantially below those based on Marcatili's method or on the slab model. As expected, however, the agreement is better for higher frequencies and for rectangular guides with higher aspect ratios. In fact, one may conclude from the above illustration that, for ribbon guide with large aspect ratios ((height/width) > 5) and for the frequency region [area$(\epsilon_1 - 1)$/(free-space wavelength)^2] > 0.3, the configuration loss factor calculated according to Marcatili's method or the slab model gives an extremely good approximation to the true value and may be readily used to design low-loss ribbon dielectric waveguides.

V. Experimental Verifications

This exceptionally low loss behavior of the dielectric ribbon waveguide supporting the dominant ${}_eHE_{11}$ mode will now be verified by measurements. A newly designed dielectric waveguide cavity resonator which is capable of supporting the dominant mode is used [10]. A schematic diagram of the measurement setup is shown in Fig. 11.

A dielectric rod resonant cavity consists of a dielectric waveguide of length d terminated at its ends by sufficiently large, flat, highly reflecting plates that are perpendicular to the axis of the guide. Microwave energy is coupled into and out of the resonator through small coupling holes at both ends of the cavity. For best results, the holes are dimensioned such that they are beyond cutoff. At resonance, the length of the cavity, L, must be $m\lambda_g/2$ (m an integer), where λ_g is the guide wavelength of the particular mode under consideration. By measuring the resonant frequency of the cavity, one may obtain the guide wavelength of that particular guided mode in the dielectric waveguide. The propagation constant, β, of that mode is related to λ_g and v_p, the phase velocity, as follows:

$$\beta = \frac{2\pi}{\lambda_g} = \frac{\omega}{v_p}. \tag{16}$$

The Q of a resonator is indicative of the energy storage capability of a structure relative to the associated energy

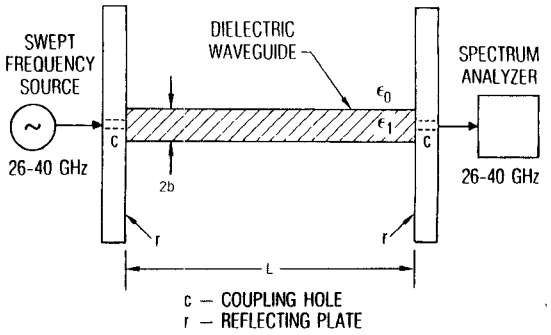

Fig. 11. A schematic diagram of the experimental setup.

TABLE II
Rexolite Strip Waveguides ($\epsilon_1 = 2.55$, $\tan\delta = 0.9\times10^{-3}$)

	$2a$ (cm)	$2b$ (cm)	a/b	L (cm)	Area (cm^2)
WG1	0.767	0.251	3.1	20.32	0.193
WG2	1.072	0.167	6.4	20.32	0.180
WG3	1.40	0.14	10.0	60.96	0.195

dissipation arising from various loss mechanisms, such as those due to the imperfection of the dielectric material and the finite conductivity of the end plates. The common definition for Q is applicable to the dielectric rod resonator and is given by

$$Q = \omega\frac{\overline{W}}{\overline{P}} \tag{17}$$

where ω is the angular frequency of oscillation, $\overline{W}$ is the total time-averaged energy stored, and $\overline{P}$ is the average power loss. Three Rexolite dielectric strip waveguides were fabricated and placed in a parallel-plate resonator. The dimensions of these waveguides are listed in Table II. The measurement procedure was described in a previous paper [10]. The coupling was such that only the dominant mode was excited, and the primary loss mechanism in the resonator was the dielectric loss. A swept signal was coupled into the cavity, and the output took the form of a series of narrow resonances; the resonant frequencies and half power bandwidths were measured with the spectrum analyzer. At each resonance the Q is given by

$$Q_m = \frac{f_m}{\Delta f_m} \tag{18}$$

where f_m is the mth resonance and Δf_m is the half-power bandwidth at that resonance. Plots of the measured Q's for these waveguides are shown in Fig. 12. As explained in [10] the primary loss mechanism in this measurement configuration is the dielectric loss, and the measured Q is the dielectric Q. For this case the relation between α and Q is [10], [14]

$$\alpha = (v_p/v_g)\beta/(2Q) \tag{19}$$

and the measured $\epsilon_1 R$ is given by

$$\epsilon_1 R = (v_p/v_g)(\beta/Q)/\left(\omega\sqrt{\mu\epsilon_0}\tan\delta\right) \tag{20}$$

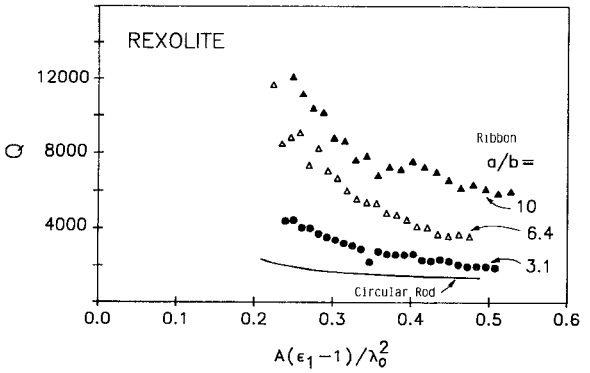

Fig. 12. Measured Q as a function of frequency for the four Rexolite waveguides. The dielectric constant and loss tangent of Rexolite are, respectively, 2.55 and 0.9×10^{-3}. Only the low-loss ${}_eHE_{11}$ mode is supported by the structure.

where β, v_p, and v_g were measured as described in [10] and $\tan\delta$ is the value previously determined for Rexolite. A plot of the external power density distribution across the three waveguides using an electric probe is shown in Fig. 13. The height of the probe was positioned such that the power level was 10 dB below the level at the surface of the waveguide. At this level the Q was not significantly affected by the presence of the probe. Plots of the external power density decay away from the surface of the waveguide are shown in Fig. 14, along with the calculated values. Plots of the measured $\epsilon_1 R$'s for the Rexolite rectangular waveguides are shown in Fig. 15 along with the calculated values for these waveguide dimensions. Excellent agreement was found for all three samples used in our experiment.

VI. Conclusion

This investigation shows that, by using a high-aspect-ratio ($a/b>10$) dielectric ribbon waveguide made with high-dielectric-constant ($\epsilon_1>9$) low-loss ($\tan\delta_1\approx10^{-4}$) material, it is possible to design an ultra-low-loss mm/sub-mm wave transmission system with the following features [15]:

- Extremely low attenuation constant for the dominant guided mode—the attenuation constant can be made lower than 10–20 dB/km in the mm/sub-mm wavelength range.
- This low-loss waveguide structure can be made with *known* low-loss dielectric material such as alumina, quartz, or sapphire—no major breakthrough in research on low-loss materials is needed to achieve the target of less than 10–20 dB/km for the attenuation constant.
- The guide can be made flexible; i.e., it can turn corners.
- The guide is economical and easy to manufacture.
- The guide is EMP resistant.
- Unlike metallic structure, this guide presents a relatively low scattering profile.

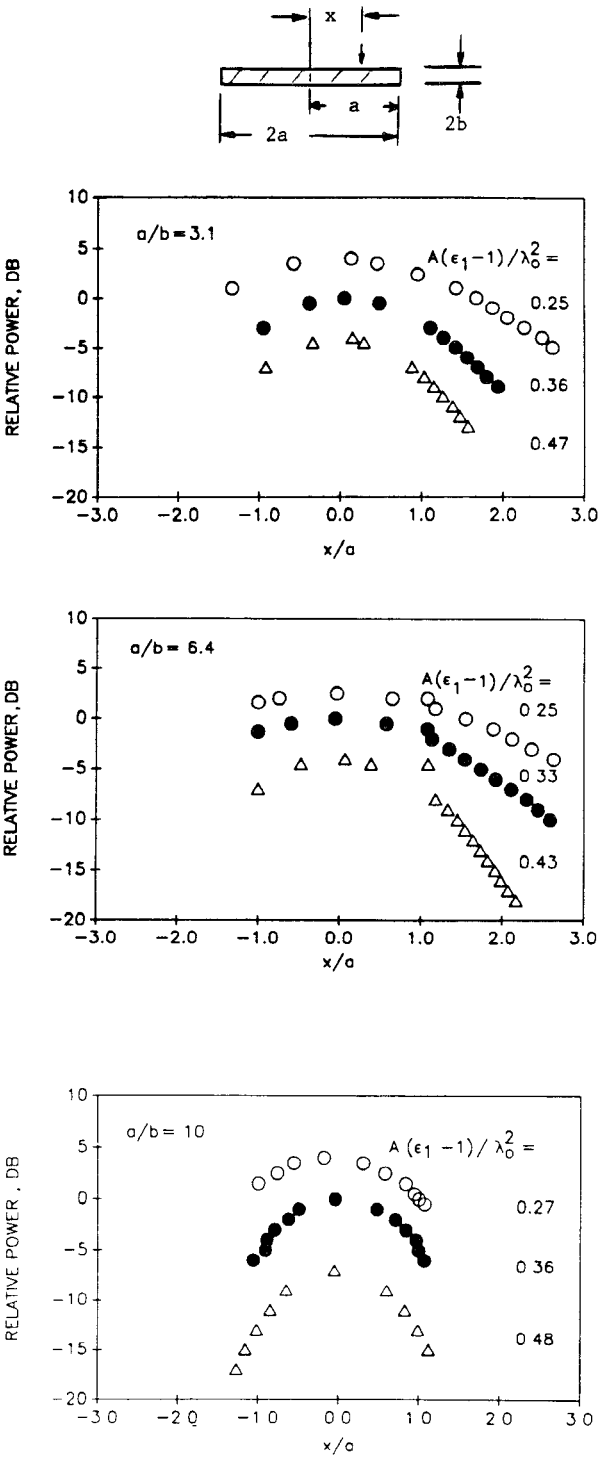

Fig. 13. External power density distribution for the guided mode for three Rexolite waveguide samples.

- It is easy to couple power into and out of the guiding structure.
- Using photolithographic techniques, circuits can be conveniently etched on waveguide surface.

Realization of our ultra-low-loss dielectric waveguide will encourage further development in the perfection of a new class of low-loss dielectric waveguides and components for use in the mm/sub-mm wavelength range.

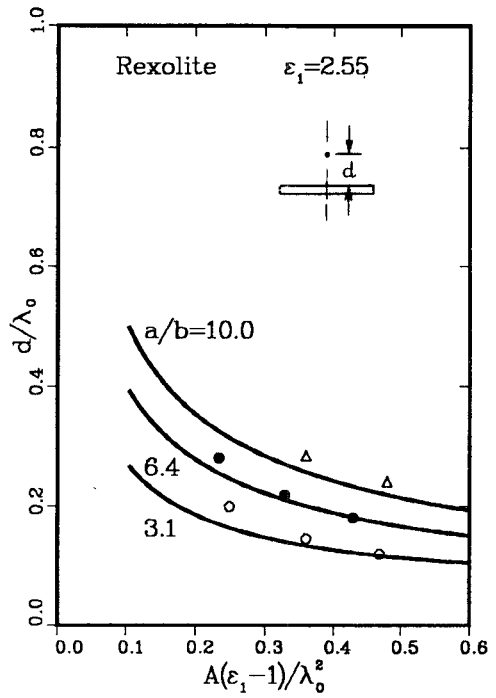

Fig. 14. External power density as a function of the normalized distance s/λ_0; s is the distance away from the surface of the guide. Solid lines are calculated results.

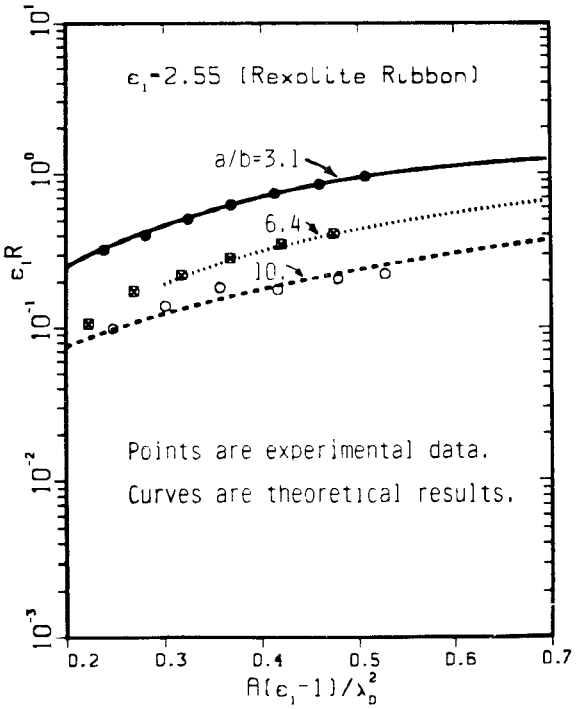

Fig. 15. Comparison between calculated configuration loss factor and measured data for dielectric ribbon waveguide with three different aspect ratios.

Acknowledgment

The authors express their gratitude to H. B. Dyson for being primarily responsible for obtaining the measurement data. They also would like to thank S. L. Johns for assisting in the measurements and plotting some of the data and G. G. Berry for fabricating the dielectric waveguides. The authors at UCLA wish to thank Dr. J. Hamada and Dr. B. Wong for their enthusiastic support of the UCLA–TRW MICRO Program.

References

[1] M. N. Afsar and K. J. Button, "Millimeter-wave dielectric measurement of materials," *Proc. IEEE*, vol. 73, pp. 131–153 1985.

[2] R. Birch, J. D. Dromey, and J. Lisurf, "The optical constants of some common low-loss polymers between 4 and 40 cm^{-1}." *Infrared Physics*, vol. 21, pp. 225–228, 1981.

[3] M. N. Afsar, "Precision dielectric measurements of nonpolar polymers in the millimeter wavelength range," *IEEE Trans. Microwave Theory Tech.*, vol. MTT-33, pp. 1410–1415, 1985.

[4] J. R. Birch and T. J. Parker, *Infrared and Millimeter Waves*, vol. 2, K. J. Button, Ed. New York: Academic Press, 1979.

[5] W. B. Bridges, "Low loss flexible dielectric waveguide for millimeter wave transmission and its application to devices," California Institute of Technology, Report No. SRO-005-1 and No. SRO-005-2, 1979–1982.

[6] W. B. Bridges, M. B. Kline, and E. Schweig, *IEEE Trans. Microwave Theory Tech.*, vol. MTT-30, pp. 286–292, 1982.

[7] S. Ramo, J. R. Whinnery, and T. VanDuzer, *Fields and Waves in Communication Electronics*, 2nd ed. New York: Wiley, 1984.

[8] E. A. J. Marcatili, *Bell Syst. Tech. J.*, vol. 48, p. 2071, 1969.

[9] C. Yeh, K. Ha, S. B. Dong, and W. P. Brown, "Single-mode optical waveguides," *Appl. Opt.*, vol. 18, pp. 1490–1504, 1979.

[10] F. I. Shimabukuro and C. Yeh, "Attenuation measurement of very low loss dielectric waveguides by the cavity resonator method applicable to millimeter/submillimeter wavelength range," *IEEE Trans. Microwave Theory Tech.*, vol. 36, pp. 1160–1167, 1988.

[11] C. Yeh, "Attenuation in a dielectric elliptical cylinder," *IEEE Trans. Antennas Propagat.*, vol. AP-11, pp. 177–184, 1963.

[12] R. E. Collin, *Field Theory of Guided Waves*. New York: McGraw-Hill, 1960.

[13] C. Yeh, "On single-mode polarization preserving multi-layered optical fiber," *J. Electromagn. Waves and Appl.*, vol. 2, pp. 379–390, 1988.

[14] C. Yeh, "A relation between α and Q," *Proc. IRE*, vol. 50, p. 2143, 1962.

[15] C. Yeh, F. I. Shimabukuro, and J. Chu, *Appl. Phys. Lett.*, to be published.

C. Yeh (S'56–M'63–SM'82–F'85) was born in Nanking, China, on August 11, 1936. He received the B.S., M.S., and Ph.D. degrees in electrical engineering from the California Institute of Technology, Pasadena, in 1957, 1958, and 1962, respectively.

He is presently Professor of Electrical Engineering at the University of California at Los Angeles (UCLA). He joined UCLA in 1967 after serving on the faculty of USC from 1962 to 1967. His current areas of research interest are optical and millimeter-wave guiding structures, gigabit-rate fiber-optic local area networks, and scattering of electromagnetic waves by penetrable, irregularly shaped objects.

Dr. Yeh is a fellow of the Optical Society of America and a member of Eta Kappa Nu and Sigma Xi.

Fred I. Shimabukuro (S'55–M'56) was born in Honolulu, HI, on September 3, 1932. He received the B.S. and M.S. degrees in electrical engineering from the Massachusetts Institute of Technology, Cam-

bridge, in 1955 and 1956, respectively, and the Ph.D. degree from the California Institute of Technology, Pasadena, in 1962.

He worked with the Hughes Aircraft Company from 1956 to 1958, and since 1962 has been at the Aerospace Corporation, El Segundo, CA. His current research activity is in millimeter- and submillimeter-wave technology.

Dr. Shimabukuro is a member of Sigma Xi.

J. Chu (S'80) was born in Taiwan on November 14, 1959. He received the B.S. degree in engineering from UCLA in 1982, and the M.S. degree in electrical engineering from the California Institute of Technology, Pasadena, in 1983. He is presently completing the requirements for the Ph.D. degree in electrical engineering at UCLA. His current research activity is in millimeter-wave guiding structures and in quantum electronics.